Optimization of Packaging Design of TWEAM Module for Digital and Analog Applications

Kwang-Seong Choi, Jong-Hyun Lee, Jiyoun Lim, Young-Shik Kang, Yong-Duck Chung, Jong Tae Moon, and Jeha Kim

Packaging technologies for a broadband and narrowband modulator with a traveling wave electro-absorption modulator (TWEAM) device were developed. In developing a broadband modulator, the effects of the device and packaging designs on the broadband performance were investigated. The optimized designs were obtained through a simulation with the result that we developed a broadband modulator with a 3 dB bandwidth of 38 GHz in the electrical-to-optical (E/O) response, an electrical return loss of less than -10 dB at up to 26 GHz, an rms jitter of 1.832 ps, and an extinction ratio of 5.38 dB in a 40 Gbps non-return to zero (NRZ) eye diagram. For analog application, the effect of the RF termination scheme on the fractional bandwidth was studied. The microstrip line with a double stub as a matching circuit and a laser trimming process were used to obtain an S_{11} of -34.58 dB at 40 GHz and 2.9 GHz bandwidth of less than -15 dB.

Keywords: Broadband and narrowband modulators, TWEAM, package resonance, double stub, laser trimming.

I. Introduction

External optical modulators are versatile in digital and analog applications [1]. They have optically-broadband characteristics so that widening the optical transmission band for wavelength division multiplexing is easily achievable in the digital area. The requirements of modulators for digital applications are a wide modulation bandwidth, high extinction ratio, low optical insertion loss, low electrical return loss, and low driving voltage. Also, their low transmission loss and compatibility with RF systems makes them useful in an RF transmission system. For analog application, the modulators should have such properties as a high link gain at the operating frequency, bandwidth, linearity, and low link noise figure [2].

We developed a traveling wave electro-absorption modulator (TWEAM) for digital and analog applications. A TWEAM is very attractive for many applications, especially at high frequency because it overcomes the bandwidth limitation of the lumped electroabsorption modulator [3]. To make real the high-speed properties of the TWEAM in a packaged module level, an optimized packaging design was developed. It is the packaging design that determines the application area of a packaged module because there is no difference in the device chip either for digital or analog applications.

In this study, the packaging technologies of the TWEAM modules for digital and analog applications were investigated. The packaging design for the digital modulator was focused on the broadband characteristics because the electrode structure of the device was a grounded coplanar waveguide (GCPW) which was vulnerable to the parallel plate mode. This mode plays the role of a resonance source [4]-[6]. The resonance suppression method was analyzed with High Frequency Structure Simulator

(HFSS) simulation and validated with the experimental measurements. From these processes, a broadband modulator without resonance was developed. For the analog modulator, to achieve a wide fractional bandwidth, the effect of the RF termination scheme was studied. The microstrip line with a double stub design was adopted as an impedance matching circuit at 40 GHz, and the laser trimming process was applied for the minimum return loss at 40 GHz. With an electrical-to-optical (E/O) response measurement, this approach was proven to be effective in obtaining an increase in the frequency response.

II. TWEAM Device and Its Characterization

The frequency response of a TWEAM is related to the structural parameters such as the epi and electrode structure. Since the epi structure directly affects the high-frequency response and extinction ratio [7], the epi-layer was carefully designed through the finite difference time domain simulation. A 0.5 μm thick n^+-layer grown on a semi-insulating InP substrate was designed for slow wave mode operation. A 0.3 μm intrinsic layer contained the strain-compensated multiple quantum well structure which consisted of thirteen pairs of wells (10 nm, −0.38 % tensile strained) and barriers (7 nm, 0.5 % compressive strained). The photo-luminescence peak was at 1.5 μm.

To study the effect of electrodes on the response, we prepared three types of devices with 100, 200, and 300 μm long active waveguides for comparison. At each side of the active waveguide was a 250 μm long passive waveguide butt-jointed. For the high-frequency operation, we employed the coplanar waveguide (CPW) electrode and formed it by evaporation. The details of the device fabrication process were presented in [8]. Figure 1 shows the schematic diagram of a TWEAM device.
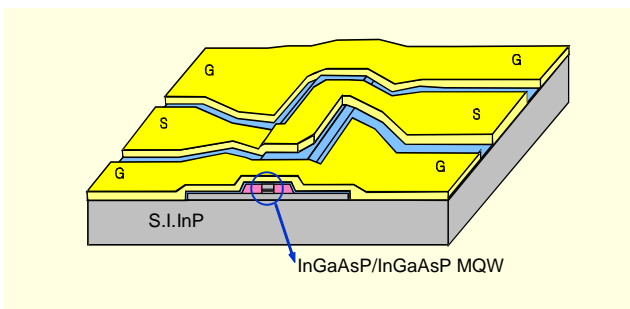

Fig. 1. Schematic diagram of TWEAM device.

For comparison, we prepared three kinds of CPW electrodes which differed in the width of the signal electrode and in the gap between the signal and ground electrodes. We observed the return loss and the insertion loss from the 100 μm long devices as presented in Fig. 2. It was found that the

S_{11} of the devices became small with the narrow electrode width. For a given width, the device exhibited a larger return loss with the wider gap. Since a narrow electrode width and a wide gap means high characteristic impedance in the CPW structure, these results agreed well with the fact that the characteristic impedance of an InP TWEAM was lower than 50 Ω [9]. On the other hand, the S_{21} was observed to be less than −2.5 dB in the range of frequency of up to 65 GHz for all the electrode structures. Figure 3 shows the characteristic impedance calculated from the measured S parameters of the fabricated devices with the electrode structure of a 6 μm width and 3 μm gap as a function of frequency. The characteristic impedance was about 30 Ω regardless of the length of the active waveguide.
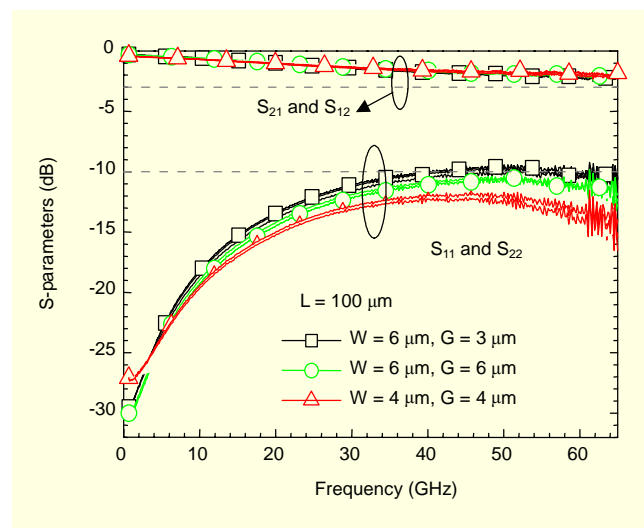

Fig. 2. Measured S parameters of fabricated TWEAM devices with various traveling wave electrode structures.
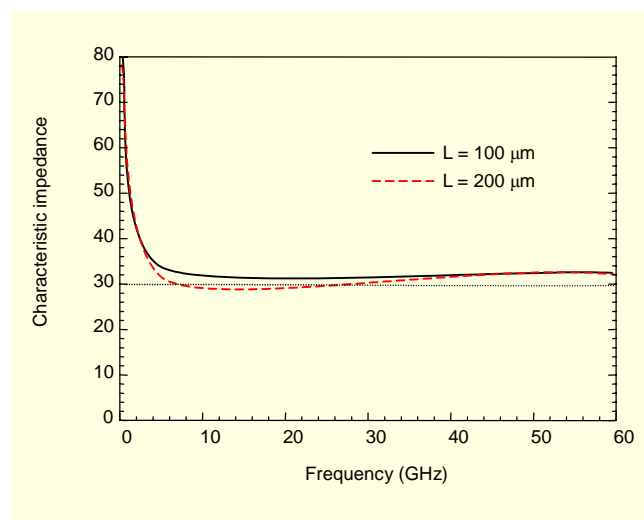

Fig. 3. Characteristic impedance of the devices with 100 μm- and 200 μm-long electrodes.

III. Packaging Design for the Broadband Module and the Performance of the Packaged Module

TWEAM modules were packaged in a butterfly-type housing with a V-connector, as shown in Fig. 4. It consists of the device, submounts, fibers, a thermoelectric cooler, a thermistor, and a V-connector. For a broadband modulator, a 50 Ω thin film termination resistor was used to obtain a large electrical return loss over a wide frequency range. The design of a feeding submount between the device and V-connector was a tapered CPW transmission line with a 50 Ω characteristic impedance. The wide section of the tapered CPW was connected to the V-connector and its narrow section was bonded by the ribbon interconnection. The narrow section is preferred in the high frequency performance because of the weak leakage coupling and radiation [5]. Vias were designed in the feeding submount to connect top grounds to the back metallization of the submount in order to suppress unwanted parallel plate modes and stabilize the coplanar quasi-TEM mode. The exact dimension and position of the vias were determined using HFSS simulation to achieve a good electrical return loss and insertion loss over the wide range of frequency.
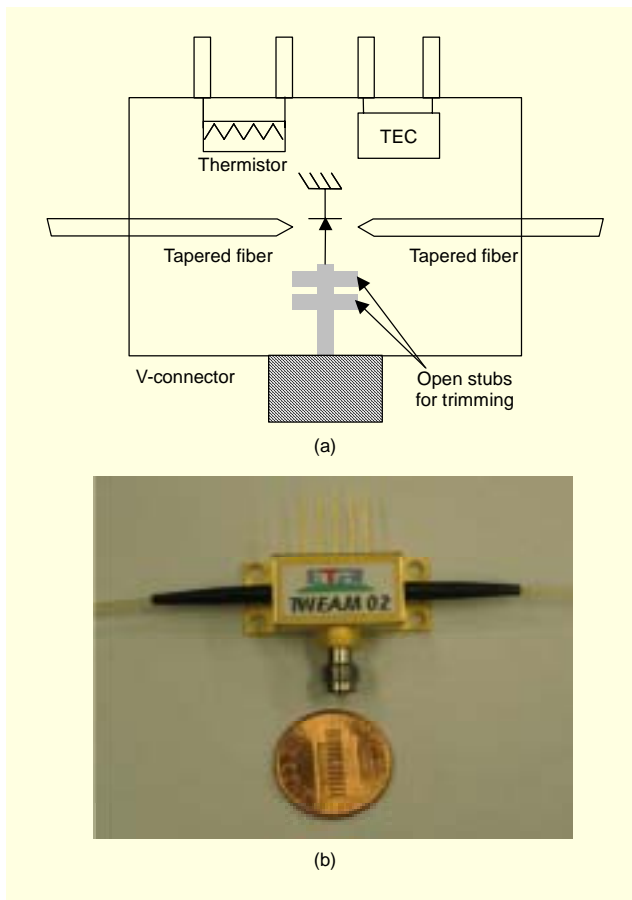
The feeding submount, the device, and the termination submount were interconnected with 2 mil.-wide gold ribbons. For the optical coupling of the device with the fibers, tapered optical fibers were actively aligned at each facet of the device. The typical insertion loss between fiber and fiber was around 12 dB.

Since the CPW structure was designed on the device, it actually formed a GCPW structure with the bottom ground of the device. The GCPW structure was reported to tend to have a parallel plate mode which can cause resonances. Usually, most coupling to parallel plate mode occurs at the input/output feeds and at the interconnections [4]-[6].

The packaged module was simulated using HFSS to check the resonance associated with the packaged structure. The device was modeled as a simple GCPW with a dielectric constant because the device properties were considered to have little effect on the resonance phenomena. Figure 5 shows the simulated return loss as a function of frequency. Sharp resonances occurred near 22 and 39 GHz. From the field distribution at the resonance frequencies, it was concluded that the resonances near 22 and 39 GHz were caused by the parallel plate mode and the cavity formed by the ceramic submount, respectively. The parallel plate mode can be suppressed by several methods: adding via holes to connect the top grounds of the CPW to the backside ground, using an additional absorbing substrate, introducing patterned backside metallization, and using integrated resistors to damp resonance [4]-[6]. Among them, we adopted the method using an additional absorbing substrate because the other methods could not be realized easily in this modulator module. The cavity resonance can be controlled with the cavity dimension and dielectric constant of the substrate material in the cavity.

Silicon was chosen as the absorbing substrate and the proper resistivity of silicon was determined using HFSS simulation.
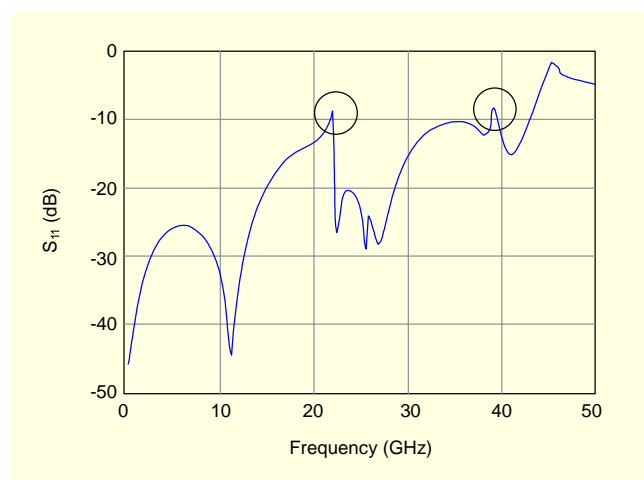

Fig. 4. (a) Structure and (b) picture of TWEAM module.

Fig. 5. Simulated return loss of the module with GCPW device.

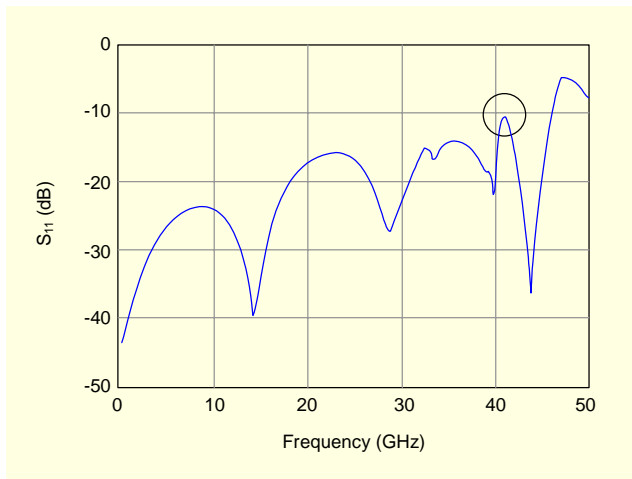Fig. 6. Simulated return loss of the modified module.

Fig. 7. Measured return loss of the module types I and II.

The proper thickness of the device was also obtained with the simulation because the silicon can increase the electrical insertion loss. For the application of the silicon block, the bottom ground on the device chip was removed and non-conductive epoxy was used to mount the silicon block between the device and ground. Figure 6 shows the simulation results of the modified packaged module. The resonance near 22 GHz disappeared. The resonance near 40 GHz was still observed but its magnitude was decreased below 10 dB because of the silicon. Its effect on the performance of the module was not considered severe because the resonance frequency was beyond the bandwidth required to meet a 40 Gbps NRZ data transmission.

Two types of packaged modules were prepared to verify the simulation results: a type I with the device having a GCPW structure, and type II with a silicon block between the device and the bottom ground. The electrical return loss and E/O frequency response were measured with an Anritsu 37397C vector network analyzer and a photodetector with the known frequency response. The electrical return losses of module types I and II with a 100 μm-long device as a function of frequency are shown in Fig. 7. The resonances at 24 GHz and 39 GHz were observed in the module type I as expected in the simulation. The amplitude of S_{11} was below −10 dB at up to 28 GHz. The module type II exhibited no resonance near 24 GHz which agreed well with the simulation result. The resonance near 39 GHz was also hidden because of the small magnitude of the resonance peak as expected in the simulation. The amplitude of S_{11} was below -10 dB at up to 26 GHz. Figure 8 shows the measured small signal E/O responses of module types I and II at the wavelength of 1550 nm with a −1.5 V bias voltage. The resonances at 24 and 39 GHz were also observed in the module type I. Similar to the measured S_{11} results, the E/O response of the module type II did not show the resonance peak. The frequency roll-off in the E/O response was observed
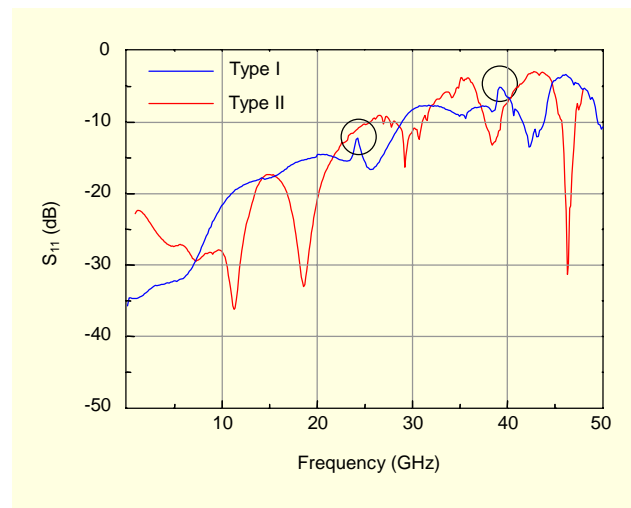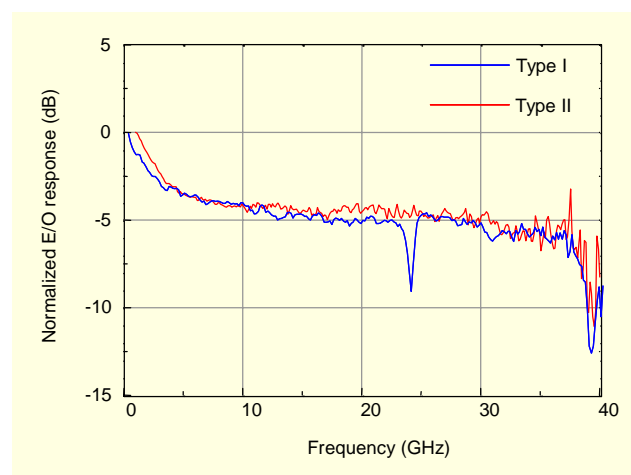

Fig. 8. Measured E/O response of the module types I and II.

at a low frequency below 4 GHz in modules I and II, which is currently under investigation. Excluding the low frequency roll-off, the small signal 3 dB bandwidth of module types I and II was about 38 GHz.

The 40 Gbps NRZ eye patterns at 1550 nm of both modules were measured. Figures 9 and 10 show the measured 40 Gbps eye patterns of modules I and II, respectively. The input optical power to the modules with a bias voltage of −1.5 V was 10 dBm. The eye opening of module type I was not clear, which was considered to be related with the optical coupling loss between the device and fibers and the package resonance. It was reported that the package resonance affected the eye opening [9]. The eye diagram of module type II showed a clear eye pattern which was achieved through enhancing the optical coupling between the device and fibers and eliminating the resonance. The rms jitter was 1.832 ps, and the extinction ratio was 5.38 dB.
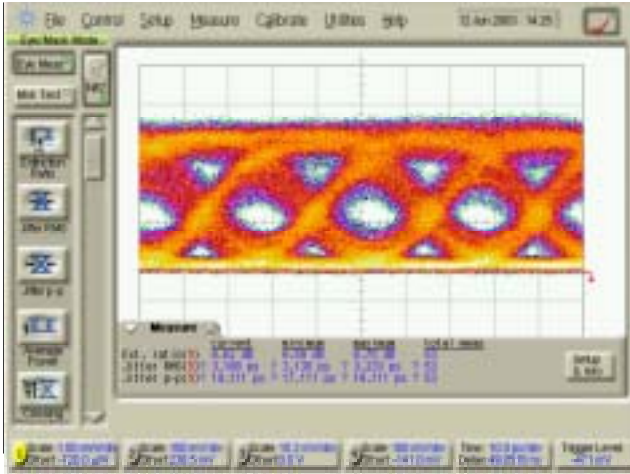
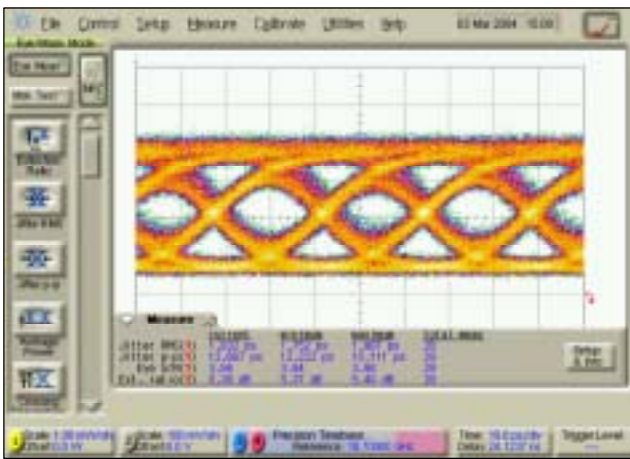Fig. 9. Measured 40 Gbps NRZ eye patterns of the module type I.

Fig. 10. Measured 40 Gbps NRZ eye patterns of the module type II.

IV. Packaging Design for the Narrowband Module and the Performance of the Packaged Module

The design of the feeding submount for a narrowband module was the microstrip transmission line with a 50 Ω characteristic impedance. Its design contained the transition between the microstrip line and the CPW because of the device structure. The microstrip had a double stub as a matching circuit to achieve the maximum electrical return loss at 40 GHz. In designing the shunt stub, the stub was balanced along the series transmission line to minimize transition interaction between the shunt stub and the series transmission line [10]. The S parameters of the device were measured to give the estimated input impedance value at 40 GHz so that HFSS simulation was utilized to design the pattern on the feeding submount.

For the RF termination of the module, any value of termination could be used as long as the reflection at the RF input port is sufficiently suppressed with the matching circuit. However, there is one design factor known as the quality factor determining the fractional bandwidth of the module. J. Lim et al. [11] reported that to obtain a wide fractional bandwidth, 30 Ω termination was preferred, which was the characteristic impedance of the TWEAM device.

To evaluate the effect of the termination, the input impedances of submodules with open and 30 Ω termination were simulated using the following process. Here, open termination was adopted for a small return loss over a wide frequency range except at 40 GHz. The simulation model contained the termination, interconnections, and part of the feeding submount. Then, the simulation results were combined with the measured S parameters of a device to give the input impedance of the submodule. Figure 11 shows the simulated input impedances of the submodules with open and 30 Ω termination at 40 GHz, respectively. From the simulation results, it can be concluded that 30 Ω termination is more appropriate to achieve the module with wider fractional bandwidth because the quality factor of the submodule with 30 Ω is smaller than that of the submodule with open termination. With HFSS simulation, the matching circuits for the submodules with open and 30 Ω termination were designed, and the return losses of the whole modules with open and 30 Ω termination were simulated, respectively, as shown in Fig. 12. The bandwidth of S_{11} of less than –15 dB of the module with 30 Ω termination is more than twice as wide as that of the module with open termination.
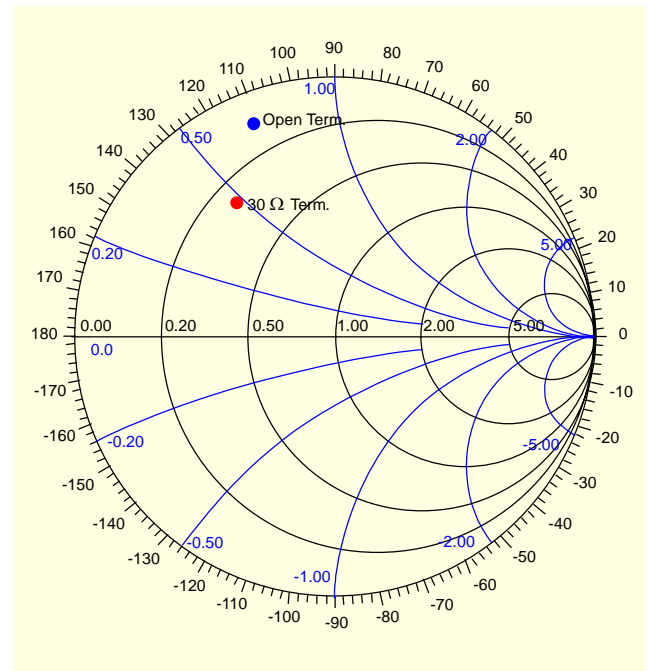

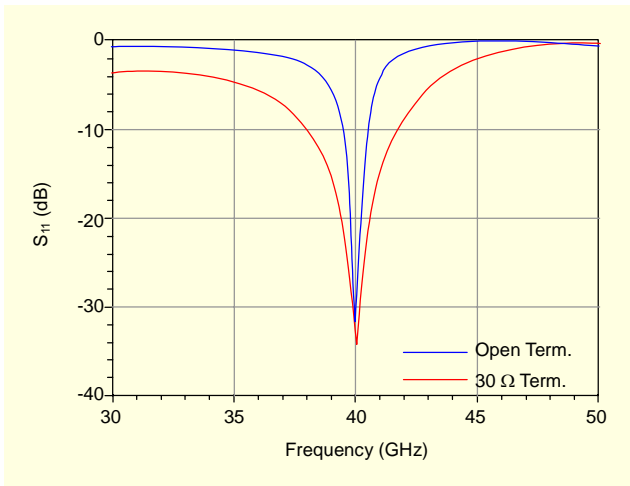Fig. 11. Simulated input impedance of the submodules with open and 30 Ω termination at 40 GHz.

Fig. 12. Simulated return loss of the modules with open and 30 Ω termination.

To verify the simulation results, two types of modules were prepared: one with open termination and the other with 30 Ω termination. The return losses of the modules were measured with an Anritsu 37397C vector network analyzer. Figure 13 shows the measured return losses of the modules. The bandwidth of S_{11} of less than –15 dB of the module with 30 Ω termination is about 2 GHz, which is twice as large as that of the module with open termination. From the results, we conclude that the simulated results agree well with the measured results and a 30 Ω termination scheme is one of the effective ways to increase the bandwidth. However, 30 Ω termination leads to the increase of the return loss at a low frequency range, so that in the system level, it can require an additional filter to cut off low frequency noise.

The proper impedance matching of a modulator at 40 GHz was performed with the laser trimming process. The laser was
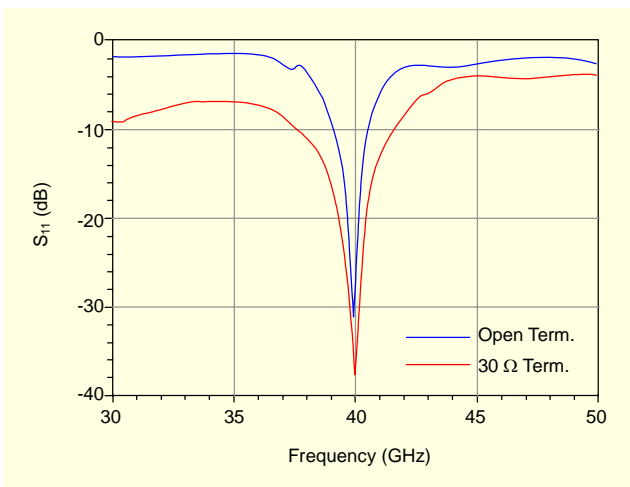

Fig. 13. Measured return loss of the modules with open and 30 Ω termination.

a Ti:Sapphire laser and was applied to the open stubs. Figure 14 shows the electrical return loss of a narrow band modulator before and after the trimming process. The S_{11} at 40 GHz after the trimming was enhanced from –10.92 to –34.58 dB. The bandwidth of S_{11} of less than –15 dB was 2.9 GHz. The bandwidth was increased due to the peak at 41.25 GHz, which was caused by λ/4 of the resonance. Figure 15 shows the E/O response of the same narrow band modulator with various bias voltages. The response shows the characteristics of the narrow band modulator as expected from the measured electrical return loss.
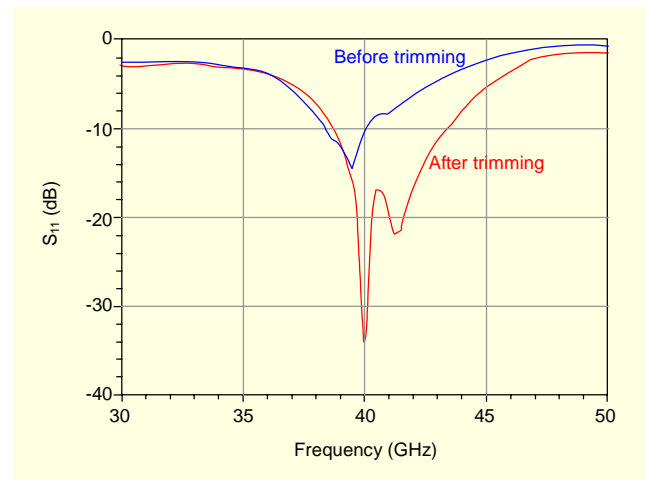

Fig. 14. Electrical return loss of a narrowband modulator before and after trimming process.
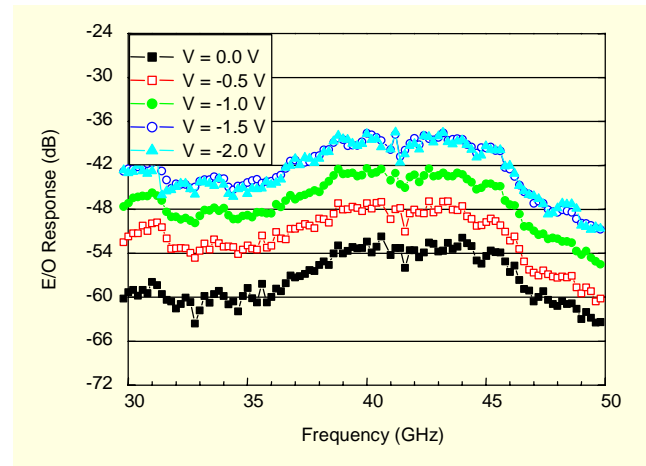

Fig. 15. E/O response of a narrowband modulator.

V. Conclusion

Packaging technologies for a broadband and a narrowband modulator with a TWEAM device were developed. A broadband modulator exhibited a 3 dB bandwidth of 38 GHz

in the E/O response, an electrical return loss of less than -10 dB at up to 26 GHz, and an rms jitter of 1.832 ps and extinction ratio of 5.38 dB in a 40 Gbps NRZ eye diagram. For analog application, 30 Ω termination was proper to obtain a wide fractional bandwidth compared with open termination. The microstrip line with a double stub as a matching circuit and the laser trimming process were used to obtain an S_{11} of -34.58 dB at 40 GHz and a 2.9 GHz bandwidth of less than -15 dB. The measured E/O response shows an increased frequency response of over 40 GHz.

References

[1] S. Kaneko, M. Noda, Y. Miyazaki, H. Watanabe, K. Kasahara, and T. Tajime, "An Electroabsortion Modulator Module for Digital and Analog Applications," *J. Lightwave Technol.*, vol. 17, no. 4, Apr. 1999, pp. 669-679.

[2] B. Liu, J. Shim, Y.-J. Chiu, A. Keating, J. Piprek, and J.E. Bowers, "Analog Characterization of Low-Voltage MQW Traveling-Wave Electroabsorption Modulators," *J. Lightwave Technol.*, vol. 21, no. 12, Dec. 2003, pp. 3011-3019.

[3] K. Kawano, M. Kohtoku, M. Ueki, T. Ito, S. Kondoh, Y. Noguchi, and Y. Hasumi, "Polarization-Insensitive Traveling-Wave Electrode Electroabsorption (TW-EA) Modulator with Bandwidth over 50 GHz and Driving Voltage less than 2 V," *Electron. Lett.,* vol. 33, Aug. 1997, pp. 1580-1581.

[4] C.– C. Tien, C.–K. C. Tzuang, S.T. Peng, and C.–C. Chang, "Transmission Characteristics of Finite-Width Conductor-Backed Coplanar Waveguide," *IEEE Trans. Microwave Theory Tech.*, vol. 41, Sept. 1993, pp. 1616-1624.

[5] S.–J. Kim, H.–S. Yoon, and H.–Y. Lee, "Suppression of Leakage Resonance on Coplanar MMIC Packages Using a Si Sub-Mount Layer," *IEEE Trans. Microwave Theory Tech.*, vol. 48, no. 12, Dec. 2000, pp. 2664-2669.

[6] B. Hou and R.W. Jackson, "Preserving Isolation in Grounded Coplanar Waveguide Circuits without Via Holes," *Electrical Performance of Electronic Packaging*, Oct. 2000, pp. 265-268.

[7] H.H. Liao, X.B. Mei, K.K. Loi, C.W. Tu, P.M. Asbeck, and W. S.C. Chang, "Microwave Structures for Traveling-Wave MQW Electro-Absorption Modulators for Wide Band 1.3 μm Photonic Link," *SPIE Optoelectron. Integrated Circuits Conf.*, vol. 3006, 1997, pp. 291-300.

[8] Y.–S. Kang, J. Lim, S.–B. Kim, Y.–D. Chung, and J. Kim, "Fabrication of Polarization Insensitive Electroabsorption Modulator with Traveling-Wave Electrode (TWEAM)," *Korea-Japan Joint Workshop Microwave Millimeter Wave Photon.*, 2003, pp. 117-120.

[9] S.–I. Kaneko, H. Itamoto, T. Miyahara, and T. Hatta, "Impact of Package Resonance on Eye Diagram in High-Speed Optical Modules," *27th European Conf. on Optical Comm.*, vol. 3, 2001, pp. 402-403.

[10] G. Gonzalez, *Microwave Transistor Amplifiers Analysis and Design*, Prentice Hall, 1997.

[11] J. Lim, Y.–S. Kang, K.–S. Choi, J.–H. Lee, S.–B. Kim, and J. Kim, "Analysis and Characterization of Traveling-Wave Electrode in Electroabsorption Modulator for Radio-on-Fiber Application," *J. Lightwave Technol.*, vol. 21, no. 12, Dec. 2003, pp. 3004-3010.

Kwang-Seong Choi received the BS degree in material science and engineering from Hanyang University, Korea, in 1993 and the MS degree in electronic material science from Korea Advanced Institute of Science and Technology, Daejeon, in 1995. From 1995 to 2001, he developed lead frame type CSPs, BLP packages, and stack packages with improving their solder joint reliability and designed high-speed electronic packages for DDR, Rambus, and RF devices for Hynix Semiconductor. He has been a Senior Research Engineer at the Electronics and Telecommunications Research Institute, Korea, since 2001, where he has been designing high-speed photonic modules over 10 GHz with electrical simulation and measurement.

Jong-Hyun Lee received the BS, MS, and PhD degrees in metallurgical engineering and materials science from Hong Ik University, Seoul, Korea, in 1995, 1997, and 2001. His doctoral work was in the electronic packaging process and soldering for SMT. He is currently a Senior Researcher in the Basic Research Lab at the ETRI. His research interests include the fabricating process for optoelectronic modules and flip-chip bonding.

Jiyoun Lim received the BS, MS, and PhD degrees in electrical engineering and computer science from Korea Advanced Institute of Science and Technology, Daejeon, in 1995, 1997, and 2002. Since 1995, she has worked on the simulation and fabrication of semiconductor optical devices. In 2002, she joined the Electronics and Telecommunications Research Institute, Daejeon, Korea, where she is a Senior Researcher. She is currently involved in a project on a 60 GHz analog optical modulator. Her research interests include the design and characterization of high-speed optoelectronic devices.

Young-Shik Kang received the BS degree in physics from Chungnam National University, Daejeon, Korea, in 1998 and the MS degree in information and communications from Kwangju Institute of Science and Technology, Kwangju, Korea, in 2000. He joined the integrated optical source team as an Investigator in a project on a 60 GHz analog optical modulator and transceiver module for RF/optic conversion at the Electronics and Telecommunications Research Institute, Daejeon, Korea, in 2001. He currently carries out research on high-speed and linear multiple quantum-well optical modulators.

Yong-Duck Chung received the BS, MS, and PhD degrees in physics from Yonsei University, Seoul, Korea, in 1995, 1997, and 2002. In 2002, he joined the Electronics and Telecommunications Research Institute (ETRI), Daejeon, Korea, where he is a senior researcher. He carried out research on an integrated WDM transmitter for metro and access networks. He is currently involved in a project on a 60 GHz analog optical modulator and transceiver module for RF/optic conversion. His research interests include the fabrication and characterization of high-speed photonic and optoelectronic devices. He also has interests in a radio-on-fiber (ROF) link wireless system.

Jong Tae Moon received the MS and PhD degrees in materials science from Hong Ik University, Seoul, South Korea in 1990 and 1995. During 1996 to 1997, he joined the Optical Module Package Team at Electronics and Telecommunications Research Institute (ETRI). During 1998 to 2000, he worked as a Team Manager in the Advanced Package Team and developed a CSP package and wafer level package for memory devices in Hyundai Electronic Company. Since 2001, he has researched an optical module package for a low cost FTTH triplexer module.

Jeha Kim received the BS and MS degrees in physics from Sogang University, Seoul, South Korea in 1982 and 1985 and the PhD degree in physics from University of Arizona, Tucson Arizona, USA in 1993. He joined Electronics and Telecommunications Research Institute, Daejeon, South Korea in 1993, where he worked at the optoelectronics section in the development of a 10 Gbit/s laser diode for optical telecommunication. During 1995 to 1998, he worked on high temperature superconducting (HTS) passive and active microwave devices for high performance wireless communications. Since 1999, he has worked on the high speed modulators and laser diodes of > 40 Gbit/s and on the narrowband RF/optic conversion devices for analog communication. He is now a project leader of 60 GHz analog optical modulator and transceiver module for RF/optic conversion. His current research interests are in the development of functional optoelectronic components and a subsystem for broadband digital and analog fiber-optic communications and radio-over-fiber (ROF) wireless link.